ACS OMEGA

Open Access

http://pubs.acs.org/journal/acsodf

Article

A Luminescent Cd-MOF Used as a Chemosensor for High-Efficiency Sensing of Fe^{3+}, Cr(IV), Trinitrophenol, and Colchicine

Xiaojing Zhou,* Lili Liu, Dongxia Wu, Yue Niu, Shimei Zheng, Jitao Lu, Yimin Feng, and Xi-Shi Tai*

Cite This: *ACS Omega* 2024, 9, 11339−11346

Read Online

ACCESS | Metrics & More | Article Recommendations | Supporting Information

ABSTRACT: A Cd-MOF was constructed based on 3,5-bis(4-carboxyphenyl) pyridine under solvothermal conditions. Its structure and phase purity were verified by single-crystal X-ray diffraction. Thereafter, some studies on the morphology, structure, and luminescent properties of the compound were carried out. The compound exhibited a highly sensitive response to Fe^{3+}, Cr(IV), trinitrophenol (TNP), and colchicine based on the fluorescence-quenching mechanism. The possible mechanism of luminescence quenching was discussed in detail.

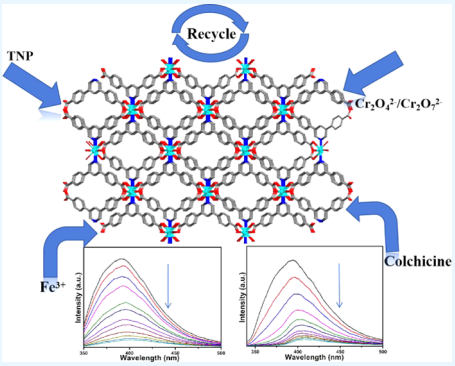

1. INTRODUCTION

Environmental pollution has grown in importance as a global concern for public health and the ecosystem over the past few decades due to social development,[1] and many types of pollutants such as nitroaromatic compounds, heavy metal ions, toxic anions, and colchicine are associated with health risks. Chemical synthesis and production of explosive materials are two common uses of nitroaromatic compounds (NACs), such as nitrobenzene (NB), 2,4,6-trinitrotoluene (TNT), and trinitrophenol (TNP), and they pose a substantial risk to human health and social security since they can contaminate air, groundwater, and soil.[2] TNP is the most dangerous among these explosives because of its tremendous explosive strength and numerous uses in dye, leather, explosive manufacturing, textile, and pharmaceutical industries.[3]

Fe^{3+} is a fundamental element that is widely distributed in ecological systems and the environment and plays a significant role in the processes of hemoglobin formation, oxygen metabolism, and electron transfer. Both an excess and shortage of iron can lead to various health problems, including reduced immunity, iron deficiency anemia, multiple organ failure, and even cancers of the esophagus and bladder.[4]

Inorganic pollutants, especially toxic anions, also pose a serious environmental hazard due to their excessive emissions from industrial facilities such as electroplating, metallurgy, etc.[5] Hexavalent chromium ions, particularly $Cr_2O_7^{2-}$ and CrO_4^{2-} anions, are extensively utilized in numerous industrial processes, including pigment printing, leather tanning, electroplating, and other associated domains. On the other hand, it has also been shown that they are two of the most dangerous pollutants in the environment. Since they can build up in living things and seriously harm human health by causing maladies such as cancers, deformities, and gene mutations, they are not easily broken down by nature. Hence, the detection of Cr(IV) is of great significance.[6]

Colchicine has also been observed to suppress many inflammatory processes (Scheme S1); it is a naturally occurring toxic compound derived initially from Colchicum spp. In humans, even minute amounts of colchicine can induce nausea, vomiting, diarrhea, and bone marrow suppression. It is also a traditional medication used to treat cirrhosis, spontaneous inflammation, and gout.[7] Therefore, the detection of colchicine is of interest.

Recently, various analytical methods have been developed and applied to identify and quantify these contaminations, and these methods primarily include spectrophotometry, inductively coupled plasma mass spectrometry (ICP-MS), gas chromatography/mass spectrometry, atomic absorption spectrophotometry (AAS), and electrochemical analysis.[8] However, these techniques are usually costly and time-consuming and require complex instruments and advanced operational skills. Therefore, there is a great need to find more effective techniques with a simple operation, fast response time, and high sensitivity. Optical sensing is well recognized as an effective, economical, and prompt detection approach, making

Received: September 25, 2023
Revised: January 21, 2024
Accepted: February 6, 2024
Published: February 29, 2024

it a viable tool for contaminant detection.[9] Luminescent metal−organic frameworks (LMOFs) are a novel family of optical materials that have experienced rapid development because of their unique photophysical characteristics, easily tailored structures, and permanent porosity, all of which fascinating properties endow them with potential applications for detecting explosives, biomolecules, gases, heavy metal ions, and solvents.[10] Nevertheless, there are very few research studies on multifunctional LMOFs for the simultaneous detection of TNP, colchicine, and metal ions. In particular, detecting trace levels of Fe^{3+}, Cr^{3+}, TNP, or colchicine in the presence of other interfering analogs is extremely challenging to accomplish selectively and sensitively.

Based on the above discussions, we herein employ 3,5-bis(4-carboxyphenyl) pyridine (H_2L) as an organic linker with Cd^{2+} to fabricate a new LMOF-CdL, denoted as compound **1**. The structure of compound **1** can be viewed as a three-dimensional network featuring one-dimensional triangular channels, which can be utilized as a multifunctional material for sensing Fe^{3+}, Cr(IV), TNP, and colchicine in methanol with high sensitivity and selectivity through effective quenching reactions.

2. EXPERIMENTAL SECTION

2.1. Physical Measurements. FT-IR spectra were acquired using a Nicolet Impact 410 FTIR spectrometer employing KBr pellets within the 4000−400 cm^{-1} spectral range. Both the excitation and emission pass widths were 2.0 nm. A 15 mL stainless steel autoclave lined with Teflon was used to perform a solvothermal reaction. C, H and N elemental studies were carried out using a PerkinElmer 2400 element analyzer. An X-ray powder diffraction (model Rigaku D/max 2550) instrument was used to acquire data for powder X-ray diffraction measurements. TGA was performed by utilizing a TGA Q500 V20.10 Build 36 instrument. The analysis was conducted from room temperature to 800 °C employing a heating rate of 10 °C/min under a flowing N_2 atmosphere. UV−vis spectra were collected at ambient temperature by using a TU-1900 spectrometer. Luminescent spectra were acquired by utilizing the FLS920 spectrofluorimeter employing excitation and emission pass widths of 2.0 nm.

2.2. Synthesis of Compound 1. Cadmium(II) nitrate tetrahydrate (15.4 mg), 3,5-bis(4-carboxyphenyl) pyridine (4.8 mg), 4,4′-bipyridine (15.6 mg), and three drops of concentrated HNO_3 were ultrasonically dissolved in DMA (5 mL), CH_3CH_2OH (2 mL), and H_2O (1 mL) in a 20 mL vial at 75 °C for 72 h. Columnar yellow crystals were then collected and washed with DMA, followed by drying at 60 °C. Yield: 58% (based on 3,5-bis(4-carboxyphenyl) pyridine); IR (KBr 4000−400 cm^{-1}): 3418 (w), 1639 (w), 1509 (s), 1598 (s), 1397 (s), 1280 (m), 1263 (w), 1011 (m), 912 (w), 855 (m), 817 (m), 779 (s), 707 (s), 669 (m), 593 (w), 526 (w), 503 (w), 486 (m). Elemental analysis (%): Calcd for $C_{25}H_{28}N_2O_7Cd$: C 51.6, H 4.82, N 4.82; found: C 51.4, H 4.84, N 4.86.

2.3. Crystal Structure Determination. The Rigaku RAXIS-RAPID, equipped with a narrow-focus, 5.4 kW sealed-tube X-ray source using graphite-monochromated Mo Kα radiation (λ = 0.71073 Å), facilitated data collection and structural analysis. The data were collected at a temperature of 20 ± 2 °C. The PROCESS-AUTO processing program was used to process the data. The direct methods of the SHELXL crystallographic software package were employed to solve the structure, and full-matrix least-squares approaches were applied to refine them on F2. Anisotropic thermal parameters were used to refine all of the compound's non-hydrogen atoms. Every hydrogen atom in the organic molecule was incorporated into the structure factor calculation geometrically. The additional crystallographic data for this study is CCDC-2205947. The atomic coordinates detailing this structure were submitted to the Cambridge Crystallographic Data Center. Since it is challenging to identify the precise solvent molecules in the structure, we further determined the molecular formula of the as-synthesized compound **1** using Platon/Squeeze, TGA, IR, and elemental analysis. The coordinates are available from the Cambridge Crystallographic Data Center (CCDC) at https://www.ccdc.cam.ac.uk/

2.4. Fluorescence Sensing Experiments. For the purpose of the fluorescence sensing tests, a mixed solution containing 3 mg of compound **1**'s milled samples and 3 mL of CH_3OH was prepared. The mixture was then sonicated for 30 min.

3. RESULTS AND DISCUSSION

3.1. Crystal Structure of Compound 1. Compound **1** is classified as a member of the monoclinic space group *I*2/*a* based on crystallographic study (Table 1). In compound **1**, the asymmetric unit has one Cd^{2+} ion and 0.5 L^{2-} ligand (Figure S1). Six carboxylate O atoms from four different L^{2-} ligands and one N atom from one L^{2-} ligand coordinate the Cd^{2+} center (Figure 1a). The L^{2-} ligand is pentacoordinated to three Cd centers, and each carboxyl group of the L^{2-} ligand adopts a double coordination pattern of $\mu 2$-$\eta 2$:$\eta 1$ (Figure 1b). The Cd−O distances vary from 2.226 (2) to 2.628 (3) Å, while the O−Cd−O angles are in the range from 53.56 to 174.25°. Additionally, the O−Cd−N angles are observed within the range of 74.82−104.65°. Both the Cd center and L^{2-} can be considered as five-coordinated nodes, resulting in the framework forming a uninodal (5,5)-connected bnn topology denoted by the point symbol of $(4^6{\cdot}6^4)$ as illustrated in Figure 2.

Table 1. Crystallographic Data and Structure Refinement Summary for Compound 1

compound	**1**
molecular formula	$C_{25}H_{28}CdN_2O_7$
formula weight	580.8
crystal system	monoclinic
space group	*I*2/*a*
a, Å	8.0481(3)
B, Å	16.0917(5)
c, Å	14.9654(5)
α, deg	90
β, deg	96.636(3)
γ, deg	90
V, Å^3	1925.15
Z	4
D_{calc}, g/cm^3	1.620
F(000)	848.0
GoF	1.073
R_1, wR_2 [$I > 2\sigma(I)$][a,b]	R_1 = 0.0308, wR_2 = 0.0863
R_1, wR_2 (all data)	R_1 = 0.0321, wR_2 = 0.0876

[a] $R_1 = \sum||F_o| - |F_c||/\sum|F_o|$. [b] $wR_2 = [\sum w(F_o^2 - F_c^2)^2/\sum w(F_o^2)^2]^{1/2}$. $w = 1/[\sigma^2(F_o^2) + (ap)^2 + (bp)]$, $p = [\max(F_o^2 \text{ or } 0) + 2(F_c^2)]/3$. a = 0.0539, b = 2.3313.

https://doi.org/10.1021/acsomega.3c07110
ACS Omega 2024, 9, 11339−11346

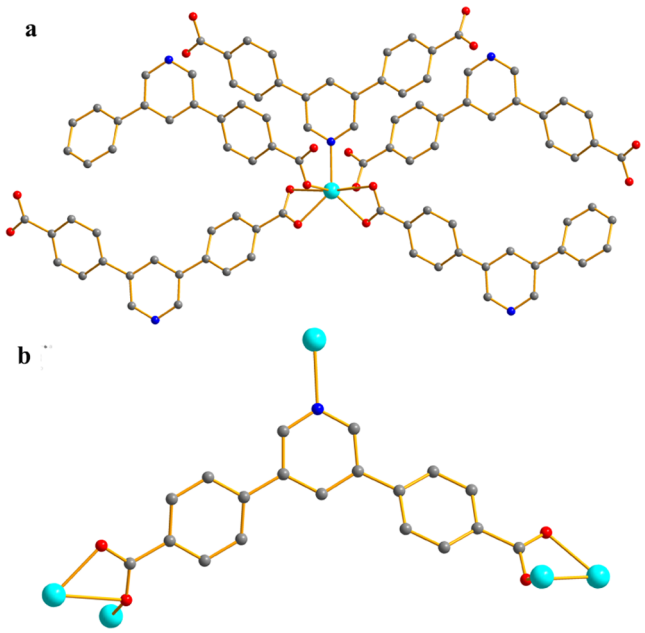

Figure 1. Coordination mode of (a) Cd center and (b) L^{2-}.

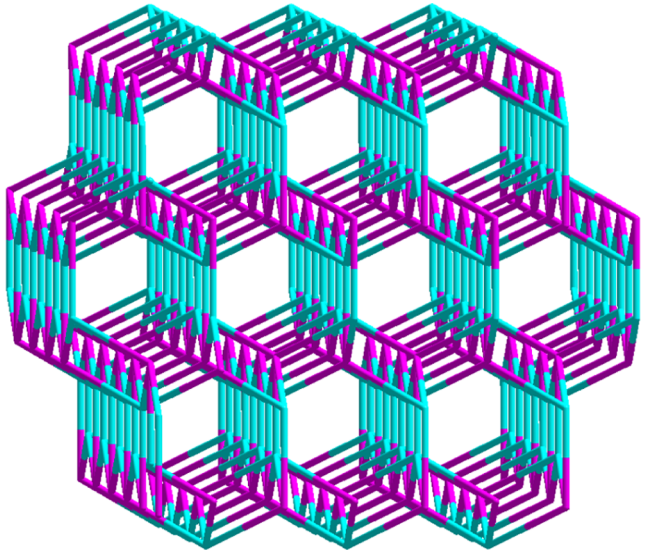

Figure 2. Topology of compound **1**.

The one-dimensional Cd-ion chains are formed by a carboxyl group bridging all of the metal ions in the structure as presented in Figure 3a. The one-dimensional Cd-ion chains then interconnect along the *b*-axis through ligands, resulting in the formation of a two-dimensional layer. This layer is then extended by Cd−N bonding, contributing to the generation of a three-dimensional framework (Figure 3b,c). Furthermore, one-dimensional ultramicroporous channels with a diameter of ∼3 Å exist along the *a*-axis, regardless of the van der Waals radius. Platon calculations reveal that the total solvent accessible volume of the 3D framework is 620.1 $Å^3$, accounting for 48.7% of the total cell volume.

3.2. Fluorescence Properties of Compound 1. The solid-state fluorescence characteristics of compound **1** and H_2L were studied at room temperature. As depicted in Figure 4, H_2L (λ_{ex} = 330 nm) obtained the maximum emission peak at 378 nm, potentially arising from $\pi \rightarrow \pi^*$ or n $\rightarrow \pi^*$ transitions. Conversely, compound **1** exhibited the maximum emission peak at 414 nm (λ_{ex} = 365 nm), which was attributed to the challenging oxidation or reduction of the Cd(II) ion because of its d10 electronic configuration. These emissions are neither MLCT nor LMCT. Thus, the emissions can be assigned to intraligand and interligand luminescence emissions. Due mostly to the ligand−metal coordination effect, compound **1**'s emissions were seen to be red-shifted when compared to free H_2L.[11]

3.2.1. Fluorescence Detection of Compound 1 in Various Solvents. The fluorescence properties of compound **1** were further tested by suspending the milled samples (3 mg in 3 mL) in various solvents like methanol, NMP (*N*-methyl-2-pyrrolidone), DMF, ethanol, DMA, DMSO, acetonitrile (CH_3CN), CH_2Cl_2, acetone, 1,4-dioxane, and H_2O, treated with ultrasonication at room temperature for 30 min. Compound **1** displayed the greatest fluorescence emission in CH_3OH, as demonstrated by Figure 5, which also confirms that compound **1**'s fluorescence intensity was significantly dependent on the solvents. Hence, in fluorescence measurements, CH_3OH was selected as the dispersion solvent.

3.2.2. Fluorescence Detection of Compound 1 in Different Cations. The determination potential of compound **1** was evaluated by sonicating 3 mg of milled samples in 3 mL of $M(NO_3)_x$ methanol solution (0.01 M) (M = K^+, Na^+, Cd^{2+}, Zn^{2+}, Co^{2+}, Cu^{2+}, Mn^{2+}, Ni^{2+}, Pb^{2+}, Fe^{3+}, Al^{3+}, Cr^{3+}, Ag^+) for 30 min to produce homogeneous suspensions. The photoluminescence response for the obtained emulsion containing different metal ions was recorded (Figure 6). The metal-ion identities play a major role in determining the fluorescence intensities. Most of the metal ions, such as K^+ and Cd^{2+}, have little effect on the fluorescence intensity of compound **1**. It is noteworthy that compound **1** exhibits a clear drop in emission intensity when Fe^{3+} is present. Additionally, Fe^{3+} demonstrates a 100% quenching, indicating that Fe^{3+} has the greatest quenching impact on compound **1**. To assess the stability of compound **1** in a methanol solution, the collapse of framework-related fluorescence quenching after sensing different metal ions is excluded according to PXRD measurement (Figure S10).

3.2.3. Fluorescence Detection of Compound 1 in Different Concentrations of Fe^{3+} Solution. To further evaluate the sensing selectivity toward Fe^{3+}, 1×10^{-3} M Fe^{3+} was prepared to test the emission response (3 mg compound **1** in 3 mL methanol), and the fluorescence intensity decreased continuously with gradually increasing concentrations of Fe^{3+} solution (Figure 7). The analysis of the quenching effect involved applying the linear Stern−Volmer (S−V) equation: $I_0/I = 1 + K_{sv}[M]$, where K_{sv} signifies the quenching constant, $[M]$ represents the concentration of metal ions, I_0 denotes the initial fluorescence intensity, and I stands for the intensities observed after the addition of Fe^{3+}. The SV plot pertaining to Fe^{3+} demonstrated an almost linear correlation, boasting a strong correlation coefficient of 0.999. The calculated slope, denoting K_{sv}, amounted to 1.1×10^4 M^{-1} (as depicted in Figure S3). Compound **1**'s luminescence intensity was nearly entirely quenched in the presence of Fe^{3+} methanol solution for a given metal ion (Figure S11). To evaluate a material's efficacy as a fluorescence sensor, it is critical to determine its limit of detection (LOD). Compound **1** has the potential to be a very sensitive fluorescent probe for Fe^{3+}, as evidenced by the limit of detection of 0.028 mM for Fe^{3+}, calculated from the equation, LOD = $3\sigma/k$.

https://doi.org/10.1021/acsomega.3c07110
ACS Omega 2024, 9, 11339−11346

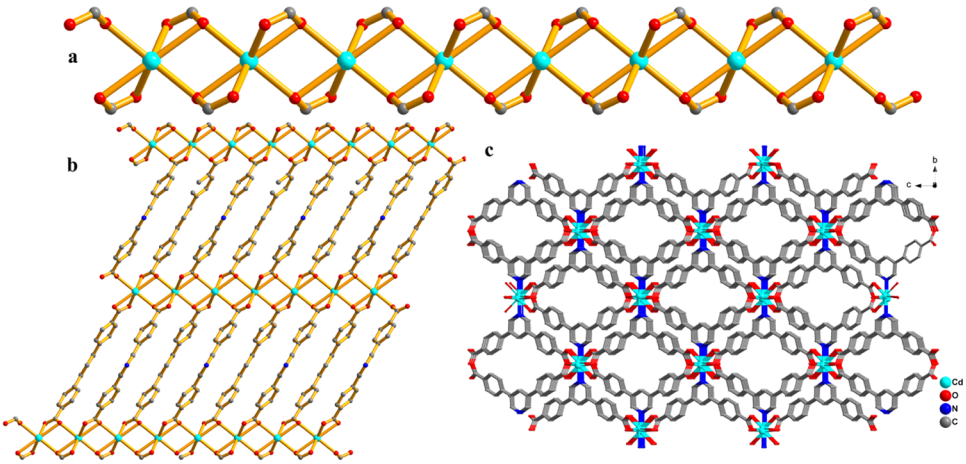

Figure 3. (a) Rod shape of the one-dimensional Cd-ion chain; (b) two-dimensional layer of compound **1** without Cd−N coordination; and (c) three-dimensional structure of compound **1**.

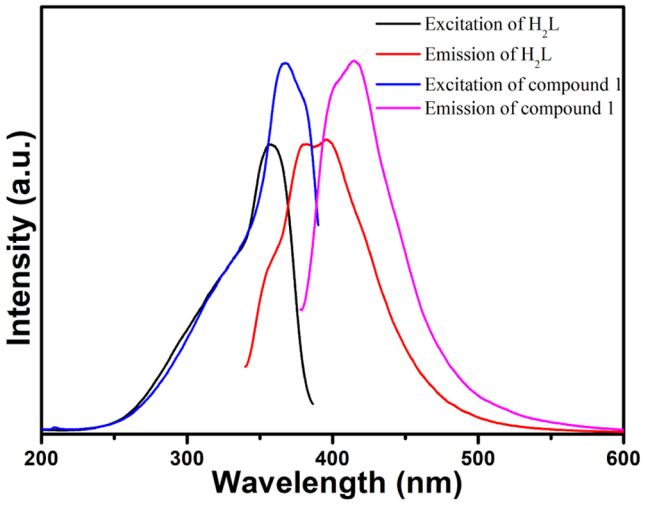

Figure 4. Solid-state fluorescence of compound **1** and H_2L.

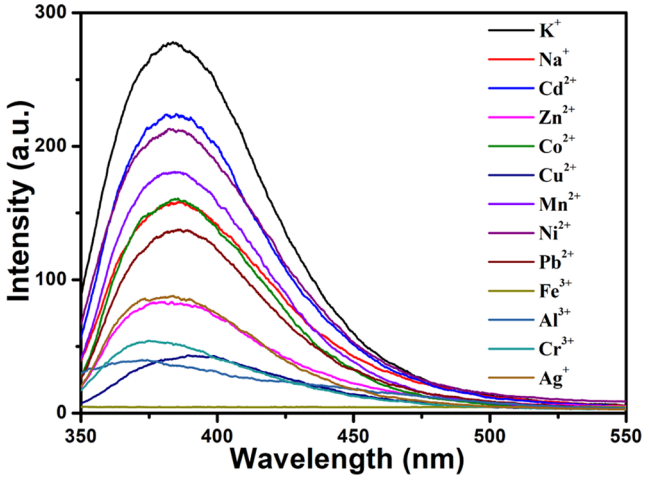

Figure 6. Fluorescence spectra of compound **1** toward different metal ions.

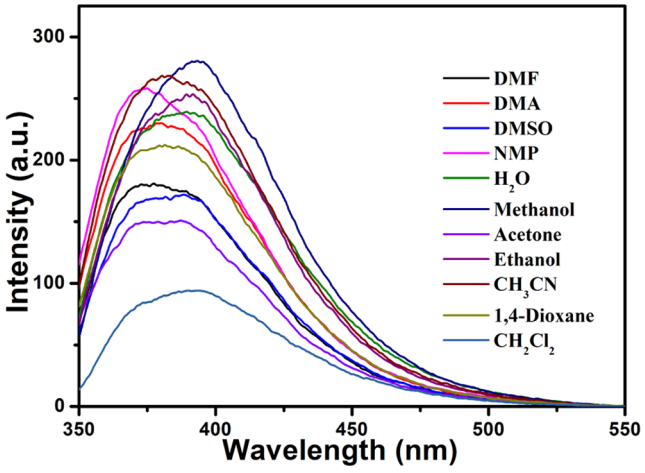

Figure 5. Fluorescence spectra of compound **1** in different solvents.

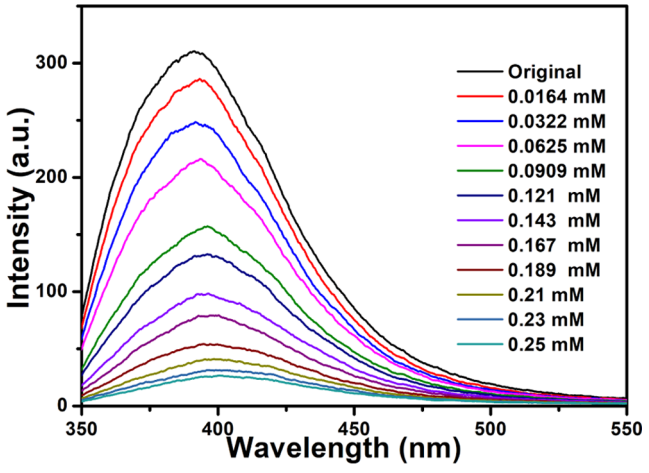

Figure 7. Fluorescence spectra of compound **1** with addition of Fe^{3+} (1×10^{-3} M).

3.2.4. Fluorescence Detection of Compound 1 in Different Anions. Experiments on anion sensing were conducted similarly to those on cation sensing. The milled sample of 3 mg compound **1** was dispersed in the individual methanol solutions of 0.01 M KX (3 mL, X^- = Br^-, I^-, NO_3^-, SCN^-, $C_2O_4^{2-}$, CO_3^{2-}, CrO_4^{2-}, $Cr_2O_7^{2-}$, SO_3^{2-}, PO_4^{3-}, Cl^-, F^-) and then subjected to 30 min of ultrasonication, after which a stable suspension was obtained for testing and investigating the fluorescence formed (Figure 8). Their fluorescence intensities

https://doi.org/10.1021/acsomega.3c07110
ACS Omega 2024, 9, 11339−11346

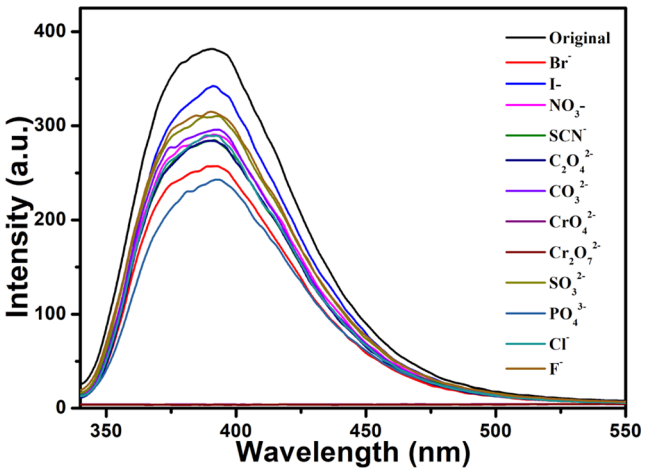

Figure 8. Fluorescence spectra of compound **1** with addition of anions (1×10^{-2} M).

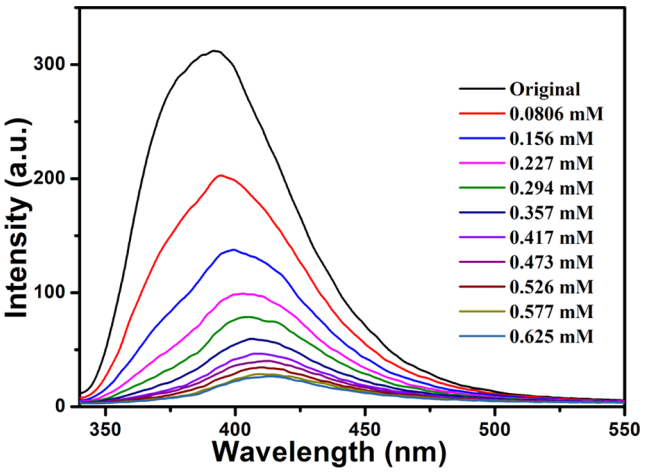

Figure 9. Fluorescence spectra of compound **1** upon adding various concentrations of $Cr_2O_7^{2-}$ (2.5×10^{-3} M).

were prominently dependent on anions. Compound **1** was primarily affected by the $Cr_2O_7^{2-}$ and CrO_4^{2-} anions, which sharply quenched the compound's fluorescence and significantly reduced it. On the contrary, the other anions showed a slight effect under the same conditions. The findings suggest that among other common anions, compound **1** could serve as a capable fluorescence sensor with excellent selectivity for Cr(VI). Competitive experiments on compound **1**'s anti-interference sensing ability provide evidence for this point. These experiments showed that compound **1**'s intensity was acutely quenched in the presence of $Cr_2O_7^{2-}$ and CrO_4^{2-} anions, but no discernible changes were seen when competitive anions were added to the corresponding solutions (Figures S12 and S13). Hence, compound **1**'s outstanding anti-interference sensing capability and high selectivity as a chemical sensor for $Cr_2O_7^{2-}$ and CrO_4^{2-} anions in methanol are amply supported by the aforementioned results.

3.2.5. Fluorescence Detection of Compound 1 in Different Concentrations of $Cr_2O_7^{2-}$ and CrO_4^{2-} Solutions. Fluorescence titration studies were conducted to examine the sensitivity during quenching. This was achieved by adding varying amounts of $Cr_2O_7^{2-}$ and CrO_4^{2-} anions. As the concentration of $Cr_2O_7^{2-}$ or CrO_4^{2-} anions increased, compound **1**'s emission intensity in methanol progressively reduced, as depicted in Figures 9 and 10, further supporting the existence of the luminescence quenching effects. According to the Stern−Volmer equation analysis, the quenching constants (K_{sv} values) for compound **1** were determined to be 1.14×10^4 M^{-1} for $Cr_2O_7^{2-}$ and 8.6×10^3 M^{-1} for CrO_4^{2-}, yielding R^2 values of 0.993 ($Cr_2O_7^{2-}$) and 0.998 (CrO_4^{2-}) (refer to Figures S6 and S7). Furthermore, the detection limits of $Cr_2O_7^{2-}$ and CrO_4^{2-} were about 16.7 and 22.1 μM, respectively, as determined by the K_{sv} values and standard deviation of the repeated fluorescence measurements of the blank solution. When compared to other MOF-based fluorescent probes, compound **1** is a superior material for Cr(VI) anion detection in methanol.[12]

3.2.6. Fluorescence Detection of Compound 1 in Various NACs. The investigation of compound **1**'s fluorescence properties aimed to discern its capability to detect NACs within a methanol solution. In this study, NACs such as 2,4-NT, 2-NT, TNP, TNT, p-NT, and NT were employed. Figure 11 shows compound **1**'s fluorescence intensity at different

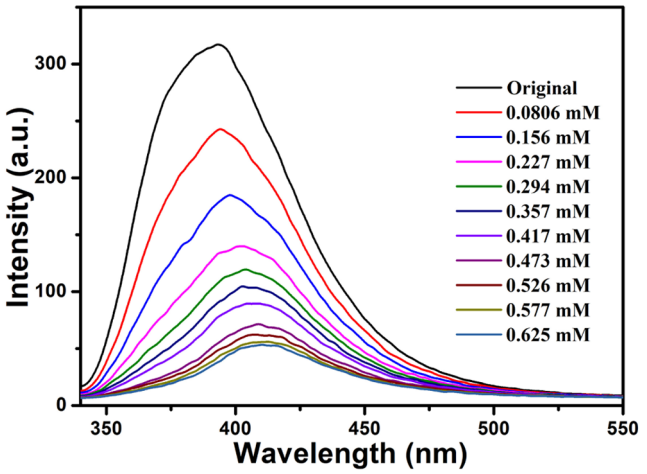

Figure 10. Fluorescence spectra of compound **1** with addition of CrO_4^{2-} (2.5×10^{-3} M).

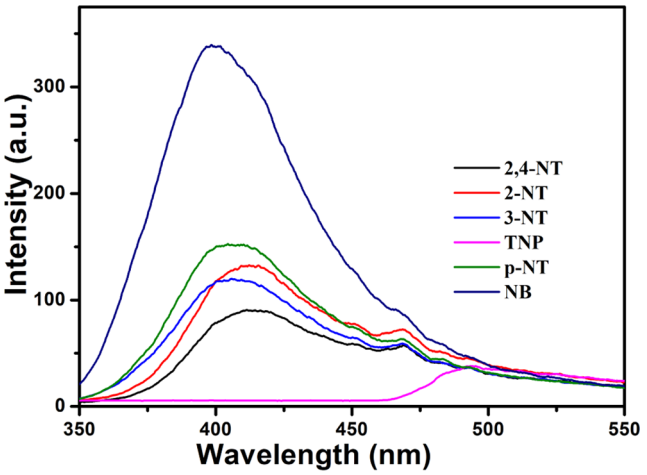

Figure 11. Fluorescence spectra of compound **1** after adding various concentrations of NACs (1×10^{-3} M).

NACs (1×10^{-3} M). The fluorescence intensity of compound **1** was continuously quenched at 385 nm, and its quenching efficiency reached 100% in a TNP methanol solution. Additionally, a highly noticeable amount of fluorescence

https://doi.org/10.1021/acsomega.3c07110
ACS Omega 2024, 9, 11339−11346

quenching was detected in this solution. Compound **1** showed minimal variation in fluorescence intensity when compared to that of the other five NACs.

3.2.7. Fluorescence Detection of Compound 1 in Different Concentrations of TNP. A fluorescence-quenching titration investigation was carried out to examine compound **1**'s sensitivity for TNP detection. TNP methanol solution (1×10^{-4} M) was gradually added to compound **1**'s suspension, resulting in a notable reduction in luminescence intensity (Figure 12). Based on the titration data, the SV curve was

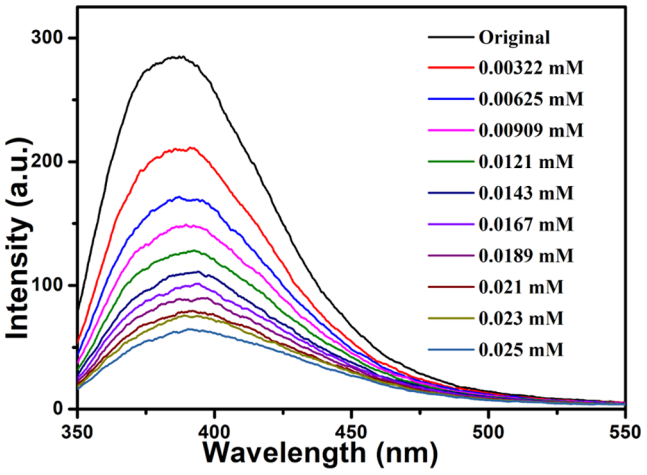

Figure 12. Fluorescence spectra of compound **1** upon addition of TNP (1×10^{-4} M).

plotted using the equation $I_0/I = 1 + K_{sv}$ [M], and a linear relationship was obtained; meanwhile, the K_{sv} of TNP was calculated as 7220 M^{-1} (R^2 = 0.9946) (Figure S4), with a detection limit of 26.3 μM, calculated using $3\sigma/k$.

3.2.8. Fluorescence Detection of Compound 1 in Different Concentrations of Colchicine. The fluorescence response of compound **1** in a methanol solution of colchicine (1×10^{-2} M) was also examined (Figure S9), and the fluorescence intensity exhibited a substantial decrease, signifying the remarkable sensitivity of compound **1** toward colchicine. Following that, a colchicine fluorescence titration investigation was carried out, in which incremental amounts of colchicine methanol solution (5×10^{-4} M) were added to the suspension of compound **1**, and there was a discernible decline in the luminescence intensity of compound **1**, as shown in Figure 13. Based on the titration data, an SV plot was acquired. The results showed that K_{sv} was equal to 4.26×10^4 M^{-1} (R^2 = 0.994) (Figure S5), and the detection limit of colchicine was 4.46 μM. These results reveal that compound **1** has a good sensitivity for the detection of colchicine in methanol.

3.3. PXRD of Compound 1. Furthermore, the recycling performance must be simple and quick. Luminescence and PXRD were used to examine the recycled samples of compound **1**, which was acquired by repeatedly washing it in methanol. Following five cycles, the luminescence intensity of compound **1** in solutions containing Fe^{3+}, Cr(IV), TNP, and colchicine was found to be nearly constant from its initial state (Figure S14), and the framework structure remained intact (Figure S15). Therefore, compound **1** is an excellent sensor for Fe^{3+}, Cr(IV), TNP, and colchicine in terms of stability and recyclability.

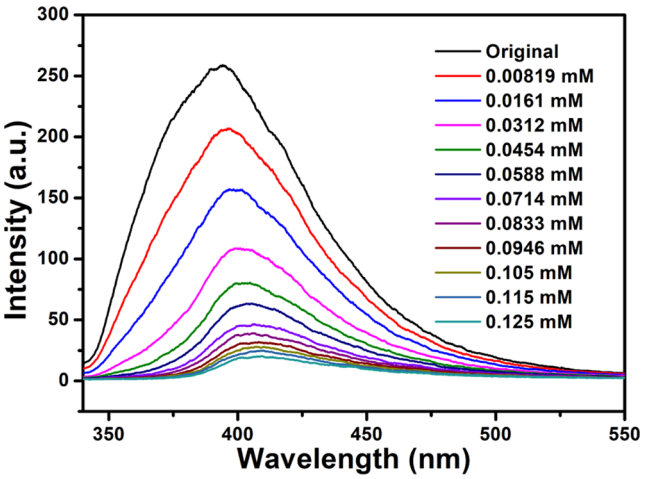

Figure 13. Fluorescence spectra of compound **1** after adding different concentrations of colchicine (5×10^{-4} M).

3.4. Fluorescence-Quenching Mechanism. Meanwhile, UV−vis absorption spectra of Fe^{3+}, Cr(IV), TNP, and colchicine depict overlaps with the luminescence excitation peak of compound **1** (Figure S8). This phenomenon indicates that the excited light's energy is absorbed by Fe^{3+}, Cr(IV), TNP, and colchicine, impeding the transfer of energy from L^{2-} to Cd^{2+} and consequently inducing the quenching effect on compound **1**, which suggested a possible energy transfer between Fe^{3+}, $Cr_2O_7^{2-}/CrO_4^{2-}$, TNP, colchicine, and compound **1**.[13]

4. CONCLUSIONS

A novel luminescent Cd-MOF was synthesized via a solvothermal method and thoroughly characterized. Luminescence sensing investigations suggest its potential as an excellent probe for highly sensitive detection of Fe^{3+}, Cr(IV), TNP, and colchicine. This flexible detection capability is greatly anticipated to offer valuable insights into the development of new multifunctional MOFs for chemical sensing.

■ ASSOCIATED CONTENT

Supporting Information

The Supporting Information is available free of charge at https://pubs.acs.org/doi/10.1021/acsomega.3c07110.

Supporting Crystallography Data (ZIP)

Table S1: selected bond distances (Å) and angles (deg) for compound **1**; Scheme S1: structure of colchicine; Figure S1: asymmetric unit of compound **1**; Figure S2: PXRD of compound **1**; Figures S3−S7: *SV* plots for luminescence intensity of compound **1**; Figure S8: UV absorption; Figure S9: fluorescence spectra of compound **1** in colchicine solution (1×10^{-2} M); Figure S10: PXRD of compound **1** and after sensing of the metal ions; Figures S11−S13: anti-interference performance of Fe^{3+}, $Cr_2O_7^{2-}$, CrO_4^{2-}; Figure S14: five cycle tests of compound **1** toward sensing Fe^{3+}, $Cr_2O_7^{2-}$/CrO_4^{2-}, TNP, and colchicine in methanol; Figure S15: PXRD patterns of the recycled compound **1** after sensing Fe^{3+}, $Cr_2O_7^{2-}$, CrO_4^{2-}, TNP, and colchicine; Figure S16: PXRD patterns of compound **1** and the luminescence intensity at three different temperatures; Figure S17: fluorescence intensity of compound **1** in K^+, Cd^{2+}, Zn^{2+}, Na^+, and Mg^{2+} methanol solutions; Figure

https://doi.org/10.1021/acsomega.3c07110
ACS Omega 2024, 9, 11339−11346

S18: TGA of compound **1**; and Figure S19: IR of compound **1**. (PDF)

AUTHOR INFORMATION

Corresponding Authors

Xiaojing Zhou − *School of Chemical & Chemical Engineering and Environmental Engineering, Weifang University, Weifang 261061, P. R. China;* orcid.org/0000-0002-9885-6549; Email: zhouxiaojing105@163.com

Xi-Shi Tai − *School of Chemical & Chemical Engineering and Environmental Engineering, Weifang University, Weifang 261061, P. R. China*; Email: taixs@wfu.edu.cn

Authors

Lili Liu − *School of Chemical & Chemical Engineering and Environmental Engineering, Weifang University, Weifang 261061, P. R. China;* orcid.org/0000-0002-3062-0783

Dongxia Wu − *School of Chemical & Chemical Engineering and Environmental Engineering, Weifang University, Weifang 261061, P. R. China*

Yue Niu − *School of Chemical & Chemical Engineering and Environmental Engineering, Weifang University, Weifang 261061, P. R. China*

Shimei Zheng − *School of Chemical & Chemical Engineering and Environmental Engineering, Weifang University, Weifang 261061, P. R. China*

Jitao Lu − *School of Chemical & Chemical Engineering and Environmental Engineering, Weifang University, Weifang 261061, P. R. China;* orcid.org/0000-0001-5167-0395

Yimin Feng − *School of Chemical & Chemical Engineering and Environmental Engineering, Weifang University, Weifang 261061, P. R. China*

Complete contact information is available at: https://pubs.acs.org/10.1021/acsomega.3c07110

Author Contributions

The experiments were conceived and designed by X.Z.; X.Z., Y.N., and D.W. carried out the experimental work; data were analyzed by L.L., S.Z., Y.F. and J.L.; supervision for this work was carried out by X.T. All authors contributed to the revision of the manuscript.

Notes

The authors declare no competing financial interest.

ACKNOWLEDGMENTS

This project was supported by the Open Project of State Key Laboratory of Inorganic Synthesis and Preparation of Jilin University 2022-34, the Shandong Provincial Natural Science Foundation (ZR2019QB011), and the Shandong Provincial Key Research and Development Program (Major Scientific and Technological Innovation Project) (No. 2019JZZY010804).

REFERENCES

(1) (a) Tyagi, D.; Wang, H.; Huang, W.; Hu, L.; Tang, Y.; Guo, Z.; Ouyang, Z.; Zhang, H. Recent Advances in Two-Dimensional Materials based Sensing Technology towards Health and Environmental Applications. *Nanoscale* **2020**, *12*, 3535−3559, DOI: 10.1039/C9NR10178K. (b) Long, C.; Jiang, Z.; Shangguan, J.; Qing, T.; Zhang, P.; Feng, B. Applications of carbon dots in environmental pollution control: A review. *Chem. Eng. J.* **2021**, *406*, 126848. (c) Wang, J.; Zhuang, S. Covalent organic frameworks (COFs) for environmental applications. *Coord. Chem. Rev.* **2019**, *400*, 213046.

(2) (a) Kovacic, P.; Somanathana, R. Nitroaromatic compounds: Environmental toxicity, carcinogenicity, mutagenicity, therapy and mechanism. *J. Appl. Toxicol.* **2014**, *34*, 10−24. (b) Sun, X.; Wang, Y.; Lei, Y. Fluorescence based explosive detection: from mechanisms to sensory materials. *Chem. Soc. Rev.* **2015**, *44*, 8019−8061. (c) Li, J.; Xiao, Y.; Shui, F.; Yi, M.; Zhang, Z.; Liu, X.; Zhang, L.; You, Z.; Yang, R.; Yang, S.; Li, B.; Bu, X.-H. Extremely Stable Sulfuric Acid Covalent Organic Framework for Highly Effective Ammonia Capture. *Chin. J. Chem.* **2022**, *40*, 2445−2450. (d) Liu, X.; Zhu, C.; Yin, J.; Li, J.; Zhang, Z.; Li, J.; Shui, F.; You, Z.; Shi, Z.; Li, B.; Bu, X.; Nafady, A.; Ma, S. Installation of synergistic binding sites onto porous organic polymers for efficient removal of perfluorooctanoic acid. *Nat. Commun.* **2022**, *13*, No. 2132. (e) Han, X.; Liu, J.; Yu, K.; Lu, Y.; Xiang, W.; Zhao, D.; He, Y. Water-Stable Eu6-Cluster-Based fcu-MOF with Exposed Vinyl Groups for Ratiometric and Fluorescent Visual Sensing of Hydrogen Sulfide. *Inorg. Chem.* **2022**, *61*, 5067−5075. (f) Dong, C.; Yang, J.; Xie, L.; Cui, G.; Fang, W.; Li, J. Catalytic ozone decomposition and adsorptive VOCs removal in bimetallic metal-organic frameworks. *Nat. Commun.* **2022**, *13*, No. 4991. (g) Zhang, Z.; Zhong, Y.; Zhang, W.; Zhao, P.; Li, H.; Liu, X. The Preparation and Application in Adsorptive Removal Hazardous Materials of MOF-Derived Materials. *J. Inorg. Organomet. Polym. Mater.* **2023**, *33*, 3315−3339, DOI: 10.1007/s10904-023-02784-9.

(3) (a) Kathiravan, A.; Gowri, A.; Khamrang, T.; Kumar, M.; Dhenadhayalan, N.; Lin, K.; Velusamy, M.; Jaccob, M. Pyrene based Chemosensor for Picric acid -Fundamentals to Smartphone device design. *Anal. Chem.* **2019**, *91* (20), 13244−13250. (b) Tanwar, A. S.; Meher, N.; Adil, L.; Iyer, P. Stepwise elucidation of fluorescence based sensing mechanisms considering picric acid as a model analyte. *Analyst* **2020**, *145*, 4753−4767. (c) Fan, Y.; Tao, T.; Wang, H.; Liu, Z.; Huang, W.; Cao, H. A Schiff base-functionalized graphene quantum dot nanocomposite for preferable picric acid sensing. *Dyes Pigm.* **2021**, *191*, 109355. (d) Pragya; Saini, V.; Rangan, K.; Khungar, B. A pyrazinium-based fluorescent chemosensor for the selective detection of 2,4,6-trinitrophenol in an aqueous medium. *New J. Chem.* **2022**, *46*, 16907−16913. (e) Zan, Y.; Kang, Y.; Wang, B.; Cui, S.; Shen, Z.; Shu, J.; Kong, X.; Chen, L.; Yan, X.; Li, Y. Amphiphilic fluorescent nanospheres for quantitative sensing of trinitrophenol in water system. *Dyes Pigm.* **2022**, *202*, 110296.

(4) (a) Doherty, C. P.; Cox, S. E.; Fulford, A. J.; Austin, S.; Hilmers, D. C.; Abrams, S. A.; Prentice, A. M. Iron Incorporation and Post-Malaria Anaemia. *PLoS One* **2008**, *3*, e2133. (b) Muñoz, M.; García-Erce, J.; Remacha, Á. Disorders of iron metabolism. Part II: iron deficiency and iron overload. *J. Clin. Pathol.* **2011**, *64*, 287−296. (c) Spottiswoode, N.; Fried, M.; Drakesmith, H.; Duffy, P. E. Implications of Malaria On Iron Deficiency Control Strategies. *Adv. Nutr.* **2012**, *3*, 570−578. (d) Wuri, H.; Ai, J.; Ga, L. Template method synthesis of highly fluorescent duplex oligonucleotide copper nanomaterials for Fe^{3+} sensing. *Mater. Res. Express* **2020**, *7*, 125001.

(5) (a) Lou, Y.; Zhao, Y.; Zhu, J. Ultrasensitive optical detection of anions by quantum dots. *Nanoscale Horiz.* **2016**, *1*, 125−134. (b) Wongkongkatep, J.; Ojida, A.; Hamachi, I. Fluorescence Sensing of Inorganic Phosphate and Pyrophosphate Using Small Molecular Sensors and Their Applications. *Top. Curr. Chem.* **2017**, *375*, 30. (c) Keefe, M. H.; Benkstein, K. D.; Hupp, J. T. Luminescent sensor molecules based on coordinated metals: a review of recent developments. *Coord. Chem. Rev.* **2000**, *205*, 201−228.

(6) (a) Wang, M.; Li, H.; Ding, X.; Jiang, L.; Wu, P.; Zheng, R.; Bao, G.; Liu, G.; Wang, J. Triphenylamine-containing imine-linked porous organic network for luminescent detection and adsorption of Cr(VI) in water. *Dalton Trans.* **2022**, *51*, 10351−10356. (b) Zhitkovich, A. Importance of Chromium-DNA Adducts in Mutagenicity and Toxicity of Chromium(VI). *Chem. Res. Toxicol.* **2005**, *18*, 3−11. (c) Kieber, R. J.; Willey, J.; Zvalaren, S. D. Chromium Speciation in Rainwater: Temporal Variability and Atmospheric Deposition. *Environ. Sci. Technol.* **2002**, *36*, 5321−5327.

(7) (a) Eleftheriou, G.; Bacis, G.; Fiocchi, R.; Sebastiano, R. Colchicine-induced toxicity in a heart transplant patient with chronic renal failure. *Clin. Toxicol.* **2008**, *46*, 827−830. (b) Peake, P. W.;

Pianta, T. J.; Succar, L.; Fernando, M.; Buckley, N. A.; Endre, Z. H. Fab fragments of ovine antibody to colchicine enhance its clearance in the rat. *Clin. Toxicol.* **2015**, *53*, 427−432. (c) Yong, J.; Tian, J.; Jiang, W.; Zhao, X.; Zhang, H.; Song, X. Efficacy of Colchicine in the Treatment of Patients With Coronary Artery Disease: A Mini-Review. *Clin. Ther.* **2022**, *44*, 1150−1159. (d) Dalbeth, N.; Lauterio, T. J.; Wolfe, H. R. Mechanism of Action of Colchicine in the Treatment of Gout. *Clin. Ther.* **2014**, *36*, 1465−1479.

(8) (a) Jha, S. K.; Yadava, R. D. S.; Hayashi, K.; Patel, N. Recognition and sensing of organic compounds using analytical methods, chemical sensors, and pattern recognition approaches. *Chemometr. Intell. Lab.* **2019**, *185*, 18−31. (b) Ghaedi, M.; Ahmadi, F.; Shokrollahi, A. Simultaneous preconcentration and determination of copper, nickel, cobalt and lead ions content by flame atomic absorption spectrometry. *J. Hazard. Mater.* **2007**, *142*, 272−278. (c) Capatina, D.; Feier, B.; Hosu, O.; Tertis, M.; Cristea, C. Analytical methods for the characterization and diagnosis of infection with Pseudomonas aeruginosa: A critical review. *Anal. Chim. Acta* **2022**, *1204*, 339696. (d) Lim, S. Y.; Shen, W.; Gao, Z. Carbon quantum dots and their applications. *Chem. Soc. Rev.* **2015**, *44*, 362−381. (e) Li, G.; Xia, Y.; Tian, Y.; Wu, Y.; Liu, J.; He, Q.; Chen, D. Review-Recent Developments on Graphene-Based Electrochemical Sensors toward Nitrite. *J. Electrochem. Soc.* **2019**, *166*, B881−B895. (f) Meng, J.; Shi, C.; Wei, B.; Yu, W.; Deng, C.; Zhang, X. Preparation of Fe_3O_4@C@PANI magnetic microspheres for the extraction and analysis of phenolic compounds in water samples by gas chromatography-mass Spectrometry. *J. Chromatogr. A* **2011**, *1218*, 2841−2847. (g) Rasheed, T.; Bilal, M.; Nabeel, F.; Adeel, M.; Iqbal, H. M. N. Environmentally-related contaminants of high concern: Potential sources and analytical modalities for detection, quantification, and treatment. *Environ. Int.* **2019**, *122*, 52−66.

(9) (a) Berhanu, A. L.; Mohiuddin, I.; Malik, A.; Aulakh, J.; Kumar, V.; Kim, K. A review of the applications of Schiff bases as optical chemical sensors. *TrAC, Trends Anal. Chem.* **2019**, *116*, 74−91. (b) Zhang, L.; Chen, X.; Wen, S.; Liang, R.; Qiu, J. Optical sensors for inorganic arsenic detection. *TrAC, Trends Anal. Chem.* **2019**, *118*, 869−879. (c) de Silva, A. P.; McCaughan, B.; McKinney, B. O. F.; Querol, M. Newer optical-based molecular devices from older coordination chemistry. *Dalton Trans.* **2003**, 1902−1913.

(10) Rasheed, T.; Nabeel, F. Luminescent metal-organic frameworks as potential sensory materials for various environmental toxic agents. *Coord. Chem. Rev.* **2019**, *401*, No. 213065.

(11) (a) Wang, H.; Qin, J.; Huang, C.; Han, Y.; Xu, W.; Hou, H. Mono/bimetallic water-stable lanthanide coordination polymers as luminescent probes for detecting cations, anions and organic solvent molecules. *Dalton Trans.* **2016**, *45*, 12710−12716. (b) Guo, X.-Y.; Dong, Z.; Zhao, F.; Liu, Z.; Wang, Y. Zinc(ii)−organic framework as a multi-responsive photoluminescence sensor for efficient and recyclable detection of pesticide 2,6-dichloro-4-nitroaniline, Fe(iii) and Cr(vi). *New J. Chem.* **2019**, *43*, 2353−2361.

(12) (a) He, H.; Chen, S.; Zhang, D.; Hao, R.; Zhang, C.; Yang, E.; Zhao, X. A micrometer-sized europium(iii)−organic framework for selective sensing of the $Cr_2O_7^{2-}$ anion and picric acid in water systems. *Dalton Trans.* **2017**, *46*, 13502−13509. (b) Ma, J.-J.; Liu, W. Effective luminescence sensing of Fe^{3+}, $Cr_2O_7^{2-}$, MnO_4^- and 4-nitrophenol by lanthanide metal−organic frameworks with a new topology type. *Dalton Trans.* **2019**, *48*, 12287−12295. (c) Parmar, B.; Rachuri, Y.; Bisht, K.; Laiya, R.; Suresh, E. Mechanochemical and Conventional Synthesis of Zn(II)/Cd(II) Luminescent Coordination Polymers: Dual Sensing Probe for Selective Detection of Chromate Anions and TNP in Aqueous Phase. *Inorg. Chem.* **2017**, *56*, 2627−2638.

(13) (a) Pal, S. C.; Mukherjee, D.; Das, M. C. pH-Stable Luminescent Metal−Organic Frameworks for the Selective Detection of Aqueous-Phase FeIII and CrVI Ions. *Inorg. Chem.* **2022**, *61*, 12396−12405. (b) Li, J.; Yu, B.; Fan, L.; Wang, L.; Zhao, Y.; Sun, C.; Li, W.; Chang, Z. A novel multifunctional Tb-MOF fluorescent probe displaying excellent abilities for highly selective detection of Fe^{3+}, $Cr_2O_7^{2-}$ and acetylacetone. *J. Solid State Chem.* **2022**, *306*, No. 122782. (c) Chen, K.; Zhang, X.; Yang, X.; Jiao, M.; Zhou, Z.; Zhang, M.; Wang, D.; Bu, X. Electronic structure of heterojunction MoO_2/g-C3N4 catalyst for oxidative desulfurization. *Appl. Catal., B* **2018**, *238*, 263−273. (d) Kavyashree, P.; Parambil, A.; Silswal, A.; Pramanik, A.; Koner, A. Trivalent metal ion sensor enabled bioimaging and quantification of vaccine-deposited Al^{3+} in lysosomes. *Analyst* **2023**, *148*, 2425−2437. (e) Parambil, A. R. U.; Kavyashree, K.; Silswal, A.; Koner, A. Water-soluble optical sensors: keys to detect aluminium in biological environment. *RSC Adv.* **2022**, *12*, 13950−13970.

https://doi.org/10.1021/acsomega.3c07110
ACS Omega 2024, 9, 11339−11346